SECOND EUROPEAN CONFERENCE ON EARTHQUAKE ENGINEERING
AND SEISMOLOGY, ISTANBUL AUG. 25-29, 2014

EMPIRICAL GREEN'S FUNCTION SIMULATION OF GROUND MOTIONS FOR THE 2013 GÖKÇEADA, TURKEY, EARTHQUAKE

Timur TEZEL[1], Hiroe MIYAKE[2] and Toshiaki YOKOI[3]

ABSTRACT

On 30 July 2013, a moderate earthquake with moment magnitude of M_w 5.0 (Global Centroid Moment Tensor) occurred in Gökçeada (Turkey)-Northern Aegean Sea. The mainshock was recorded by 58 strong motion stations operated by the Prime Ministry Disaster and Emergency Presidency (AFAD) Earthquake Department. Around 40 aftershocks were recorded by AFAD within initial 24 hours. We performed the empirical Green's function method (EGFM) to simulate the strong ground motion of this event and the largest aftershock of local magnitude M_w 4.0 using strong ground motion data.

INTRODUCTION

The Gökçeada earthquake occurred at 05:33 (UT) on 30 July 2013 in North Aegean Sea that was located at westernmost part of Turkey. The Centroid Moment Tensor (CMT) solution indicates that this earthquake is a strike-slip faulting event with a moment magnitude of 5.0. Aftershock distribution is useful to determine the source fault plane. Aftershock distribution which recorded by the two organisation does not fully show the main fault plane, so, we were unable to determine the source fault plane.

Turkey is located in the seismically active Alpine-Himalayan belt. The collision of Arabian, African and Eurasian plates is a main actor of this complex tectonic structure (Figure 1). These movements were resulted with strike-slip faulting and subduction zone and back-arc spreading in and around Anatolia. Within this tectonic frame, Anatolian plate moves to westward at rates of 20-25cm/y (Şengör et al, 1985; McClusky et al., 2000). The Gökçeada Island comprises 2 km thick sedimentary strata underlain by metamorphic rocks which are similar to those observed 170 km to the north in the Strandzha-Rhodope Mountains. Gökçeada Island is in proximity to the western part of the North Anatolian Fault Zone (NAFZ). Further southwest, this zone extends off-shore to a deep channel known as the North Aegean Trough (Roussos and Triantafyllos, 1991). In the Gulf of Saros north of Gökçeada Island, the NAFZ exhibits an extensional character attributed to a releasing fault bend geometry, and the region is considered to have been undergoing subsidence in association with the development of the fault (Tüysüz et al., 1998; Okay et al., 1999, Saatçılar et al., 1999). Studies also showed compressional tectonics for this region (Seeber et al., 2004). The island contains a set of faults in a NE-SW orientation that runs nearly parallel to the NAFZ (Koral et al., 2008).

[1]Assistant Professor, Department of Geophysical Engineering, Çanakkale Onsekiz Mart University, Çanakkale, Turkey, Email : timurtezel@comu.edu.tr
[2] Assistant Professor, Earthquake Research Institute, University of Tokyo, Tokyo, Japan, Email : hiroe@eri.u-tokyo.ac.jp
[3] Director, International Institute of Seismology and Earthquake Engineering, Building Research Institute, Tsukuba, Japan, Email : tyokoi@kenken.go.jp

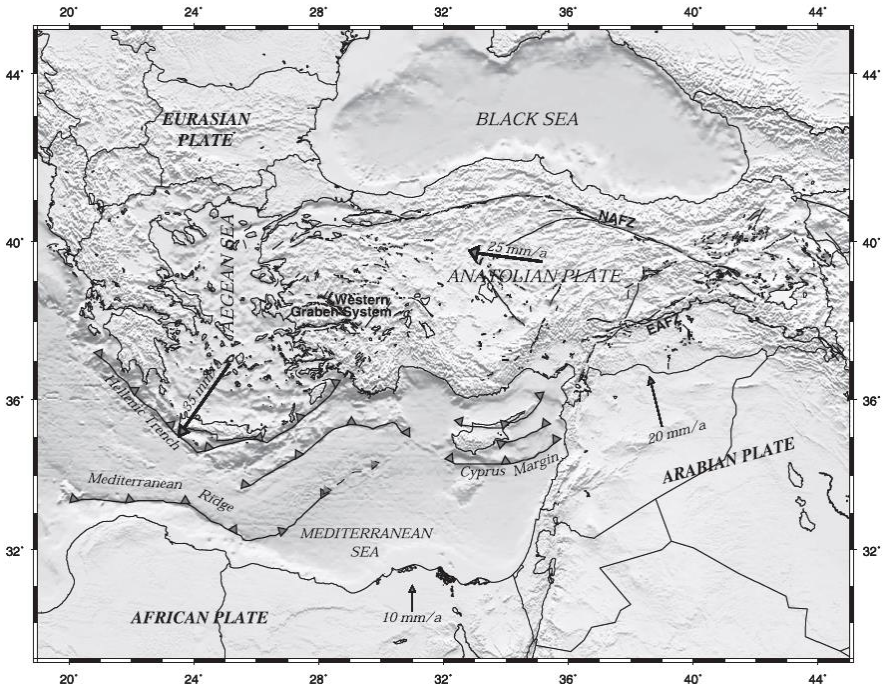

Figure 1. Tectonic setting of Turkey and surrounding regions. EAFZ: East Anatolian Fault Zone, NAFZ: North Anatolian Fault Zone, The fault data are from Şaroğlu et al. (1992).

METHOD

The empirical Green's function is a useful tool to estimate ground motions for a large earthquake using small earthquake records. The basic idea of the empirical Green's function method is small events have already been included propagation path and local site effects. Simulations were achieved by the method of Irikura (1986) which essentially uses the small events as the empirical Green's function and sums up to follow the scaling law based on the omega-square model. The source model is assumed to have a homogeneous stress drop and rise time with radial rupture propagation from the starting point. The main assumption is that the strong ground motion is generated only from rectangular shaped strong motion generation area and each area has a nearly uniform stress drop. The strong motion generation area is subdivided to N x N small elements so as to match the size of the small event which is used as the empirical Green's function. For the simulation, we used shear wave velocity from Tezel et al. (2013) who studied crustal velocity model through the Anatolia.

Seismic moment scaling parameter N and stress drop ratio C between large and small events are calculated through the ratio of flat levels of acceleration displacement spectra. Site and propagation path effects are already included in the original waveforms which are used as the empirical Green's functions. The accurate location of mainshock and aftershock is important factor as well as focal mechanism solution to observe good simulation results.

The empirical Green's function method takes in on two scaling relations between a large and a small earthquake. These are scaling relations of source parameters and scaling relations of the source spectra. In the first scaling relations, fault parameters studied by Kanamori and Anderson (1975) are expressed as the following;

$$\frac{L}{l} = \frac{W}{w} = \frac{T}{\tau} = \left(\frac{M_0}{m_0}\right)^{1/3} = N \qquad (1)$$

where L and l are fault length, W and w are fault width, T and τ are slip duration time, M_0 and m_0 are seismic moment for small and large earthquakes respectively. If the stress drop correction factor between the large and the small event is not constant, Eq. 1 must be modified by the stress drop correction factor with Eq. 2.

$$C = \frac{\Delta\sigma_L}{\Delta\sigma_S} \tag{2}$$

$\Delta\sigma_L$ and $\Delta\sigma_S$ are the stress drop correction factor for the large and small events, respectively. Then we can obtain new relation according to stress drop correction factor as Eq. 3.

$$\frac{L}{l} = \frac{W}{w} = \frac{T}{C\tau} = \left(\frac{M_0}{Cm_0}\right)^{1/3} = N \tag{3}$$

The second scaling relations are represented by the ω^{-2} source spectra scaling model studied by Aki (1967) and Brune (1970). If the average stress drop correction factor is independent of seismic moment M_0, self-similarity exist among earthquakes (Aki, 1967), the corner frequency is proportional to $M_0^{1/3}$. Then the spectral relationship between large and small events,

$$\frac{U_0}{u_0} = \frac{M_0}{m_0} = CN^3, \qquad \frac{A_0}{a_0} = CN \tag{4}$$

where, U_0, u_0, A_0 and a_0 are flat levels of displacement spectra and flat level of acceleration spectra for large and small events, respectively (Figures 2d and 2e).

For the formulation of the simulation, we need to perform the simulation of the strong motion from the large event using the record of a small event as an empirical Green's function,

$$U(t) = \sum_{i=1}^{N}\sum_{j=1}^{N}\frac{r}{r_{ij}}F\left(t - t_{ij}\right) * (C.u(t)) \tag{5}$$

where,

$$t_{ij} = \frac{r_{ij} - r_0}{V_s} + \frac{\xi_{ij}}{V_r} \tag{6}$$

Observed record from a small event is regarded as an empirical Green's function, and it summed by following Eq. 5 with time delay according to the scaling law and fault rupture process. The formulation for the EGF method by Irikura (1986) is based on the deterministic kinematic source model. The source effect of the model is characterized by five parameters in Eqs. 5 and 6: fault length (L and l), fault width (W and w), final offset-slip (r and r_{ij}), rise time (t and t_{ij}) and rupture velocity (V_r).

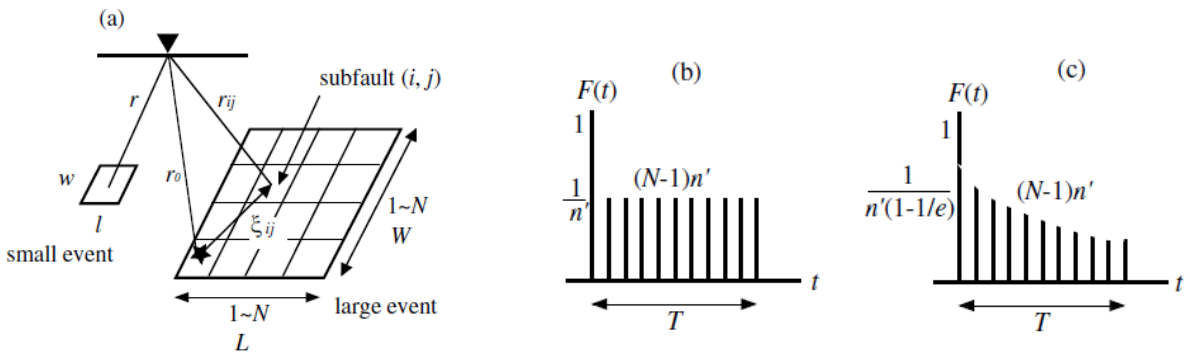

Figure 2. Schematic illustrations of the empirical Green's function method. (a) Fault areas of large and small events are defined to be L x W and l x w, respectively. (b) Filtering function $F(t)$. (c) Modified filtering function (after Miyake et al., 2003).

$U(t)$ is the simulatd waveform for the large event, $u(t)$ is the observed waveform for the small event, *N* and *C* are the ratios of the fault dimensions and stress drops between the large and small events and * shows the convolution. *F(t)* is the filtering function (correction function) to adjust the difference in the slip velocity time functions between the large and the small events. V_s and V_r are the S-wave velocity near the source area and the rupture velocity on the fault plane. *T* is the rise time for the large event, and defined as duration of filtering function *F(t)* (Figures 2b and 2c). It corresponds to the duration of slip time function on sub fault from the beginning to the time before the tail starts. Figure 2a shows the other parameters of the empirical Green's function method.

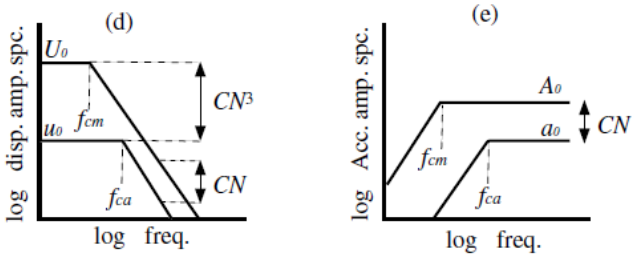

Figure 2. Schematic illustrations of (d) displacement and (e) acceleration amplitude spectra following the omega-squared source model (after Miyake et al., 2003).

DATA

The main shock of the Gökçeada Island earthquake (30 July 2013, M_w 5.0) was recorded by 58 accelerograph stations of the AFAD. Strong ground motion stations are equipped by the Guralp-CMG-TD and GMSplus. Maximum Peak Ground Acceleration (PGA) value is about 87 cm/s^2 observed at the Gökçeada Island station and its epicentral distance is about 16 km. At the other stations observed acceleration value was less than 10 cm/s^2. After the main shock about 40 aftershocks was recorded in 24 hours by the AFAD and three of them had magnitude of 4. We selected 31 July 2013 event as an element event which was a moment magnitude of 4. Main and element events were recorded by the 15 strong motion stations. Table 1 shows the focal parameters of the selected events. For this study, we used National Strong Motion Network (AFAD) seismic stations and data (Figure 3). Most stations have average shear wave velocity of the top 30 m is around 300 m/s.

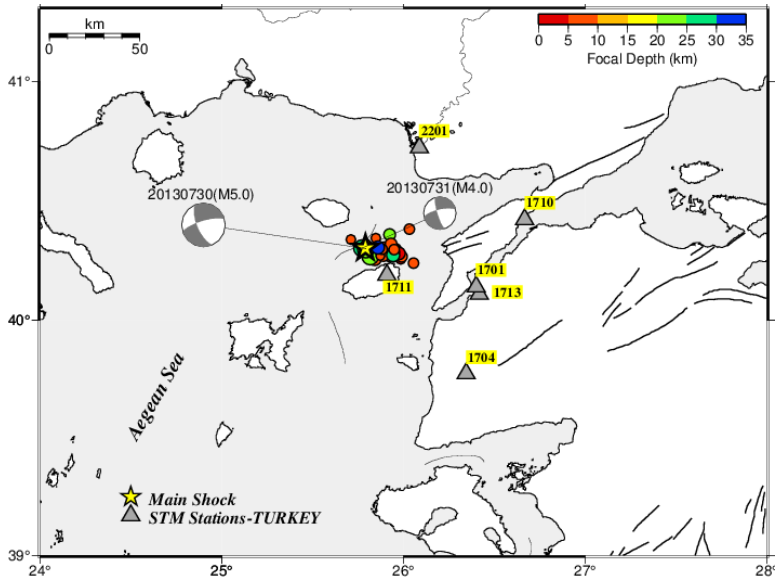

Figure 3. Location of the Gökçeada earthquake and strong motion stations indicated by yellow star and triangles, respectively. The target and element event focal mechanisms also indicated

Epicenter location and focal mechanism solution were used from Global Centroid Moment Tensor Catalogue (GCMT). Analysing of the aftershocks which were recorded by the Kandilli Observatory (KOERI) and AFAD, they showed different fault plane direction. For this reason we used EMSC aftershock data which were located using different seismic networks and we employed Joint Hypocenter Determination (JHD) technique to relocate these events. As a result aftershock data show NE-SW direction of fault plane.

Table 1. Earthquake Parameters

Event Name	Origin Time (UT)	Hypocenter Location			M_w	Focal Mechanism		
		Lat (N°)	Long (E°)	Depth (km)		Str.(°)	Dip (°)	Rake (°)
Mainshock (30/07/2013)	05:33:09.6	40.26	25.82	12	5.0	142	53	-36
Element event (31/07/2013)	01:27:04.7	40.30	25.77	26.7	4.0	163	78	-19

RESULTS

Focal mechanism of the M_w 5.0 earthquake was reported by several agencies. The fault plane solution determined by GCMT indicates that the rupture was a right lateral strike slip (strike/dip/rake: 142°/53°/-36°). However, aftershock distribution did not show purely dipping fault plane, therefore we used two fault plane values to simulate. None of the planes were not reflect dipping direction significantly and we relocated aftershock events using the Joint Hypocenter Determination (Hurukawa, 1995) which were located by the Eastern Mediterranean Seismological Center (EMSC) to capture the dipping direction.

For the empirical Green's function simulation of ground motions, *N* and *C* values were determined as 2 and 8.5, respectively using all the waveform at each station. Other simulation parameters such as size and rupture starting point of strong motion generation area, rise time, rupture velocity are determined by the trial and error calculations. An average rupture velocity value of 3.1 km/s was considered. From the N value, we divided the possible estimated strong ground motion generation area of the fault into 2 x 2 cells. Each cell on the estimated strong ground motion generation area symbolized element earthquake with stress drop correction factor C. We estimated dimensions (*l* and *w*) of the element earthquake and position of rupture starting point by doing calculation for each cell of proposed for cells for the mainshock. After some variations we figure out that the best position for rupture starting point is located in the cell (1, 2) by visually checking the fitting of the observed and synthesized motion records (Figure 4). We applied the procedure for the other stations and same results were observed.

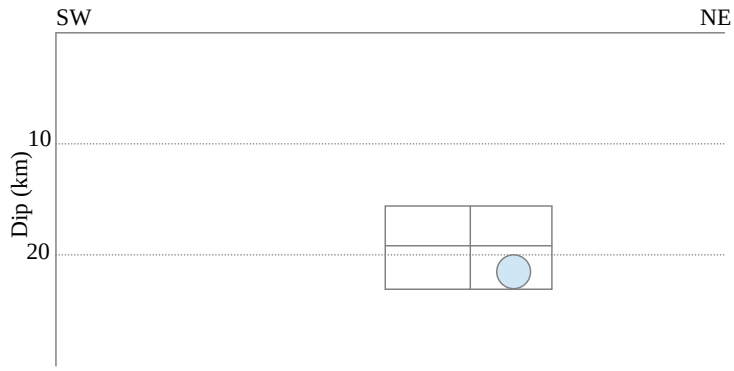

Figure 4. Source parameters of the mainshock. Coloured dot shows the rupture starting point.

For the simulation, we used shear wave velocity from the previous receiver function study of Tezel et al. (2013) who studied velocity structure model beneath the many broad-band seismic stations. Source parameters used in the simulation are listed in Table 2. Any changes of the location of strong motion generation area caused a large variability in peak values and shape of waveforms. The size of strong motion generation area for the mainshock was estimated to be 1.5 km in length by 0.8 km in width.

Table 2. Estimated Source Parameters of the Strong Motion Generation Area for the Mainshock

Event	C	N	L (km)	W (km)	S (km^2)	Vr (km/s)	Vs (km/s)
Mainshock	8.5	2	1.5	0.8	1.2	3.1	3.8

Figure 5 compares the observed and synthesized strong ground motion waveforms which were recorded at 1704 and 1711 strong motion stations.

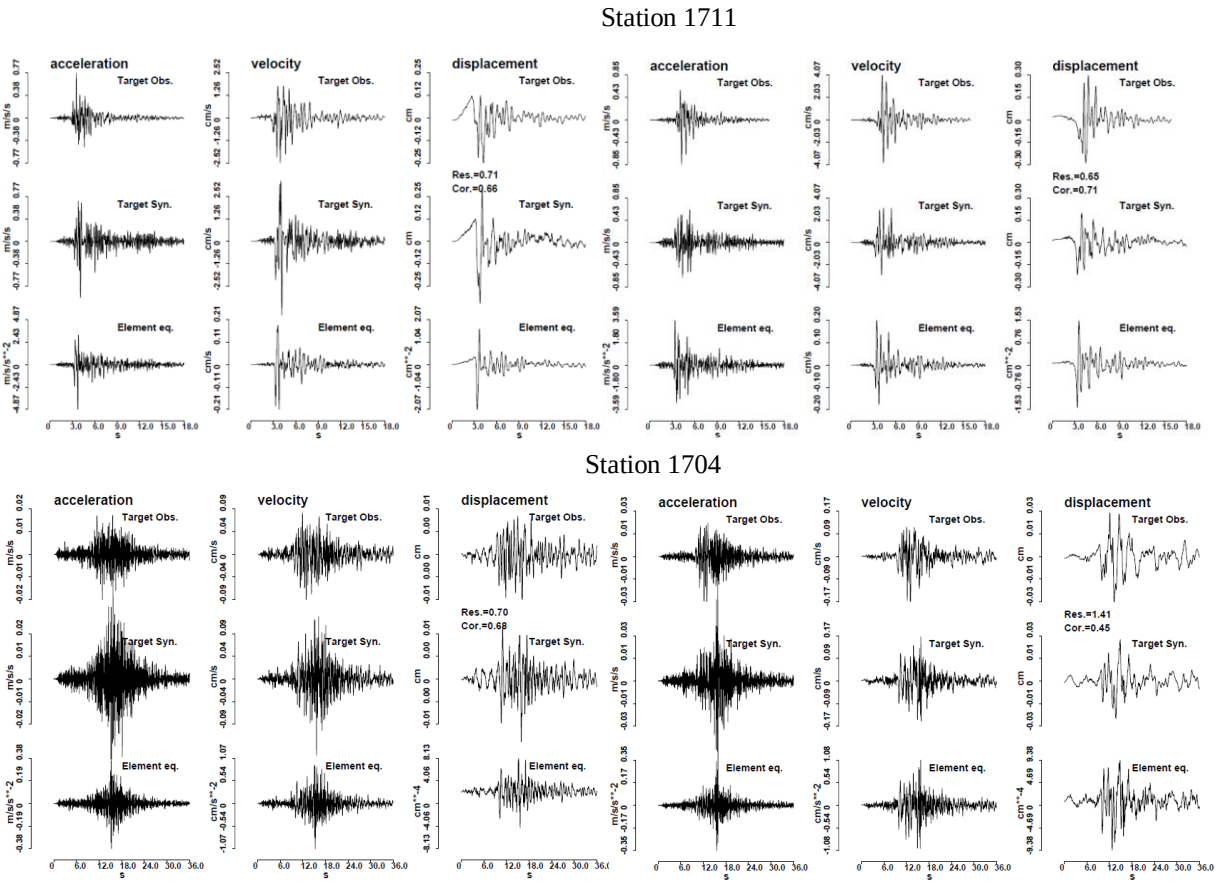

Figure 5. Comparison of observed and synthetic waveforms for the mainshock at 1704 and 1711 stations. Left and right panels show EW and NS components, respectively.

CONCLUSIONS

We estimated the source models of the mainshock (M_w 5.0) using the Empirical Green's function method. We used an element earthquake for the empirical Green's function that was a moment magnitude of 4.0. We estimated N scale parameter and C stress drop parameters using empirical Green's function using acceleration and displacement spectra. *N* value shows the scaling factor of mainshock that is referring to number of the subfaults and estimated as 2. So, we divided the strong motion generation area 2 x 2 cells. Each cell on the estimated strong ground motion generation area indicated by the element earthquake with *C*. Table 2 shows the results for the mainshock. We estimated dimensions (length and width) of element earthquake and starting point of rupture by trial operations. The size of strong motion generation area for the mainshock was estimated to be 1.5 km in length by 0.8 km in width. The rupture starting point at the northeast bottom of the estimated strong ground motion generation area with a depth about 20 km and propagated to south-westward with the velocity of 3.1 km/s that is about 80 % about of shear wave velocity. Comparison of the stations which were recorded both of the element and main events show that the waveforms of some stations could not good fit between observed and synthetics. This result mainly caused by the soil structure beneath the seismic stations that we know that mostly layers beneath seismic stations have about V_s of 300 m/s for the top 30 m depth.

REFERENCES

Hurukawa N (1995) "Quick aftershock relocation of the 1994 Shikotan earthquake and its fault planes", Geophysical Research Letters, 22, 3159-3162

Irikura K (1986) "Prediction of strong acceleration motions using empirical Green's function". Proceedings of the 7th Japan Earthquake Engineering Symposium, 10-12 December.151-156

Koral H, Öztürk H, Hanilçi N (2009) "Tectonically induced coastal uplift mechanism of Gökçeada Island, Northern Aegean Sea, Turkey," Quaternary International, 197, 43-54

McClusky S, Balassanian S, Barka A, Demir C, Ergintav S, Georgiev I, Gurkan O, Hamburger M, Hurst K, Kahle H, Kastens K, Kekelidze G, King R, Kotzev V, Lenk O, Mahmoud S, Mishin A, Nadariya M, Ouzounis A, Paradissis D, Peter Y, Prilepin M, Reilinger R, Sanlı I, Seeger H, Tealeb A, Toksoz M.N, Veis G (2000) "Global positioning system constraints on plate kinematics and dynamics in the eastern Mediterranean and Caucasus," Journal of Geophysical Research, 105, 5695‑5719

Miyake H, Iwata T, Irikura K (2003) "Source characterization for broadband ground-motion simulation: Kinematic heterogeneous source model and strong motion generation area," Bulletin of the Seismological Society of America, 93, 2531-2545

Okay A.I, Demirbağ E, Kurt H, Okay N, Kuscu I (1999) "An active, deep marine strike-slip basin along the North Anatolian Fault in the Turkey," Tectonics, 18, 129-147

Roussos N and Triantafyllos L (1991) "Structure of the central North Aegean trough: An active strike-slip deformation zone," Basin Research, 3, 39-48

Saatçılar R, Ergintav S, Demirbağ E, İnan S (1999) "Character of active faulting in the North Aegean Sea," Marine Geology, 160, 339-353

Seeber L, Emre Ö, Cormier M.H, Sorlien C.C, McHugh Polonia A, Ozer N, Çağatay N (2004) "Uplift and subsidence from oblique slip: the Ganos-Marmara bend of the North Anatolian Transform, Western Turkey," Tectonophysics, 391, 258-293

Şengör A.M.C., Görür N., Şaroğlu F (1985) "Strike-slip faulting and related basin formation in zones of tectonic escape: Turkey as a case study", in: Biddle K.T., Christie-Blick N. (Eds.), Strike-slip Faulting and Basin Formation. Soc.Econ. Paleontol. Mineral. Sp. Pub. 37, 227-264

Tezel T, Shibutani T, Kaypak, B (2013) "Crustal thickness of Turkey determined by receiver function," Journal of Asian Earth Sciences, 75, 36-45

Tüysüz O, Barka A, Yiğitbaş E (1998) "Geology of the Saros graben and its implications for the evolution of the North Anatolian Fault in the Ganos-Saros region, northwestern Turkey," Tectonophysics, 293, 105-126